iScience

CellPress
OPEN ACCESS

Article

CRISPR/Cas12a-mediated labeling of MET receptor enables quantitative single-molecule imaging of endogenous protein organization and dynamics

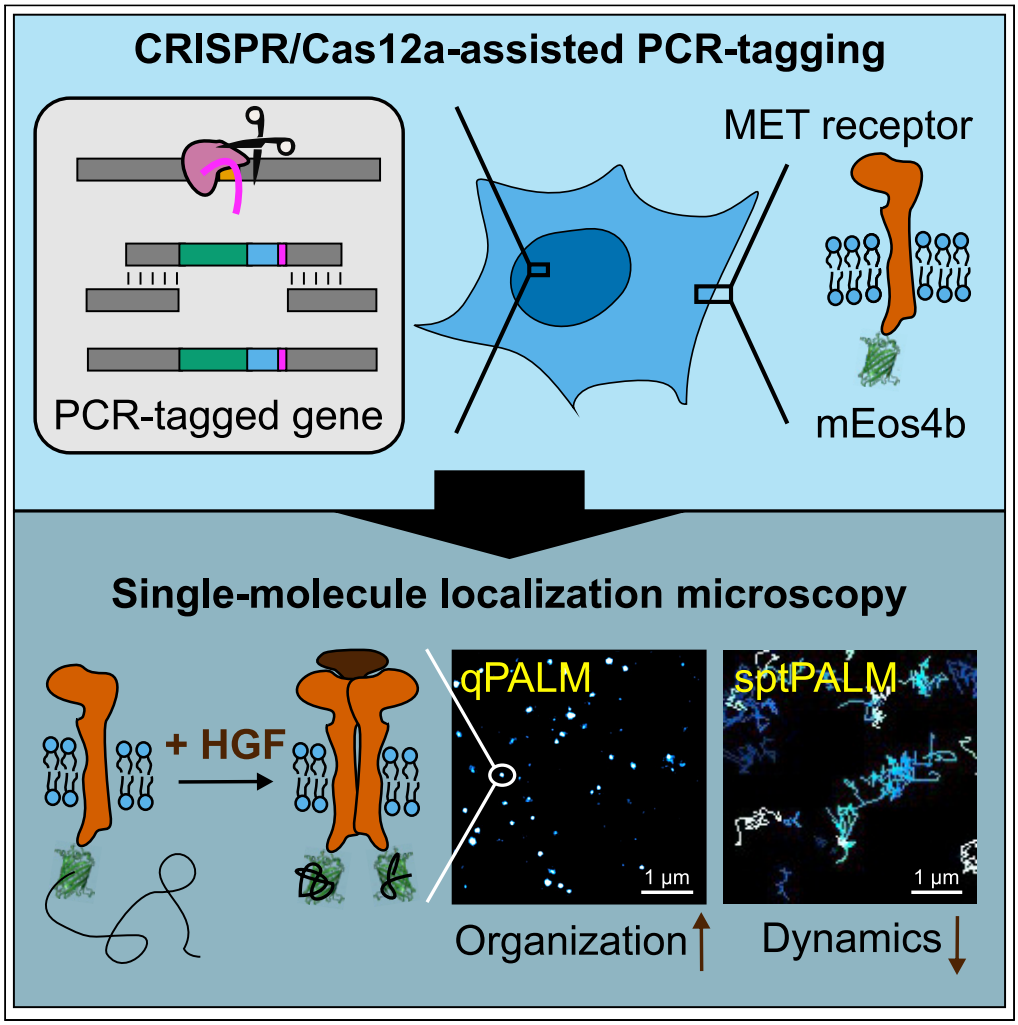

Tim N. Baldering, Christos Karathanasis, Marie-Lena I.E. Harwardt, ..., Michael Knop, Marina S. Dietz, Mike Heilemann

heileman@chemie.uni-frankfurt.de

HIGHLIGHTS

CRISPR/Cas12a enables endogenous protein labeling for super-resolution microscopy

HEK293T cells were generated with MET endogenously labeled with mEos4b

Quantitative PALM microscopy reports efficient dimerization of MET receptor

Single-particle tracking shows increased MET immobilization upon ligand treatment

Baldering et al., iScience 24, 101895
January 22, 2021
https://doi.org/10.1016/j.isci.2020.101895

iScience

CellPress
OPEN ACCESS

Article

CRISPR/Cas12a-mediated labeling of MET receptor enables quantitative single-molecule imaging of endogenous protein organization and dynamics

Tim N. Baldering,[1] Christos Karathanasis,[1] Marie-Lena I.E. Harwardt,[1] Petra Freund,[1] Matthias Meurer,[2] Johanna V. Rahm,[1] Michael Knop,[2,3] Marina S. Dietz,[1] and Mike Heilemann[1,4,*]

SUMMARY

Single-molecule localization microscopy (SMLM) reports on protein organization in cells with near-molecular resolution and in combination with stoichiometric labeling enables protein counting. Fluorescent proteins allow stoichiometric labeling of cellular proteins; however, most methods either lead to overexpression or are complex and time demanding. We introduce CRISPR/Cas12a for simple and efficient tagging of endogenous proteins with a photoactivatable protein for quantitative SMLM and single-particle tracking. We constructed a HEK293T cell line with the receptor tyrosine kinase MET tagged with mEos4b and demonstrate full functionality. We determine the oligomeric state of MET with quantitative SMLM and find a reorganization from monomeric to dimeric MET upon ligand stimulation. In addition, we measured the mobility of single MET receptors *in vivo* in resting and ligand-treated cells. The combination of CRISPR/Cas12a-assisted endogenous protein labeling and super-resolution microscopy represents a powerful tool for cell biological research with molecular resolution.

INTRODUCTION

Super-resolution microscopy enables the investigation of protein organization and dynamics at the nanoscale and opens the door for a molecular view on protein function in cells (Schermelleh et al., 2019). Single-molecule localization microscopy (SMLM) is a super-resolution technique that generates images from stochastic activation and detection of single fluorescent emitters (Sauer and Heilemann, 2017). SMLM can report on molecule numbers, simultaneously providing access to quantitative information on how proteins assemble in a cell (Dietz and Heilemann, 2019). Photoactivated localization microscopy (PALM) is a variant of SMLM that uses photoactivatable or photoconvertible fluorescent proteins that are activated stochastically by irradiation with violet light (Betzig et al., 2006). Fluorescent proteins allow stoichiometric labeling by genetic coupling to a target protein, which avoids unspecific labeling as it can occur with fluorophore-labeled antibodies. In addition, fluorescent proteins allow targeting intracellular proteins and protein domains without the need of cell membrane permeabilization which may induce damage to cellular structures (Whelan and Bell, 2015).

Several options of tagging target proteins with fluorescent proteins are available. Plasmids encoding fusion proteins can be produced synthetically in a short time and introduced into mammalian cells, e.g., by transfection. Transfected cells typically show a range of protein expression levels, which is particularly interesting for the analysis of diseases such as cancer that are associated with overexpression. However, if healthy conditions are to be studied, an endogenous expression level of the protein of interest is required (Lisenbee et al., 2003; Doyon et al., 2011; Gibson et al., 2013). For this purpose, For this purpose, a fluorophore label is favored that assures an endogenous expression level of the labeled protein in the cell.

The emergence of CRISPR/Cas as a genetic engineering tool enabled stoichiometric labeling of endogenous proteins (Deltcheva et al., 2011; Le Cong et al., 2013; Ran et al., 2013; Ratz et al., 2015). Genetic insertions of, e.g., fluorescent proteins by CRISPR/Cas9 can be performed by transfecting cells with a plasmid that codes for the Cas9 enzyme, the crRNA, and the tracrRNA. In addition, a homology template containing the DNA sequence of the fluorescent tag and homology sequences of the gene of interest are required. Using this workflow, CRISPR/Cas9 was used for protein labeling in combination with super-resolution

[1]Single Molecule Biophysics, Institute of Physical and Theoretical Chemistry, Goethe University Frankfurt, Max-von-Laue Str. 7, 60438 Frankfurt, Germany

[2]Center for Molecular Biology of Heidelberg University (ZMBH), 69120 Heidelberg, Germany

[3]German Cancer Research Center (DKFZ), 69120 Heidelberg, Germany

[4]Lead Contact

*Correspondence: heileman@chemie.uni-frankfurt.de

https://doi.org/10.1016/j.isci.2020.101895

microscopy of mostly intracellular proteins (Ratz et al., 2015; Cho et al., 2016; Hansen et al., 2017; Khan et al., 2017, 2019). However, all these studies use Cas9 for genetic editing and require time-consuming preparation of homology templates. Recently, the enzyme Cas12a was discovered, which has several advantages over Cas9. Cas12a has a higher specificity *in vivo* (Kleinstiver et al., 2016; Kim et al., 2017) and a simpler crRNA structure in comparison to Cas9 (Zetsche et al., 2015). Additionally, Cas12a cuts at some distance from the recognition sequence, resulting in more frequent cuts as the recognition sequence is not destroyed (Zetsche et al., 2015; Moreno-Mateos et al., 2017). Despite numerous advantages of CRISPR/Cas (Yamamoto and Gerbi, 2018), genetic insertions with standard CRISPR/Cas methods are time intense. Taking advantage of the CRISPR/Cas12a system, a new genome engineering approach was introduced (termed termed polymerase-chain reaction [PCR] tagging) which represents a time-saving method to generate the homologous template required for gene insertion (Füller et al., 2020). The main advantage of this technique is the fast generation of the homology template (PCR cassette) by a single PCR reaction using primers (which provide the homology arms) that can be designed with an online tool (www.pcr-tagging.com). Compared to Cas9, the Cas12a enzyme requires only one crRNA that is expressed from a gene located on the PCR cassette. Generation of a gene-specific PCR cassette (by PCR) is thus quick and it can then directly be transfected into cells together with a Cas12a expression plasmid. The crRNA is expressed from the PCR cassette and can thus together with the Cas12a enzyme produce the site-specific DNA cut. The DNA cut is then repaired by homology directed repair of the PCR cassette, which labels the protein of interest with the desired tag. This makes PCR tagging a simple and time-efficient alternative for gene labeling with which high labeling efficiencies are achieved (Füller et al., 2020).

Here, we employ PCR tagging and demonstrate almost complete labeling of the receptor tyrosine kinase MET with the photoconvertible fluorescent protein mEos4b (Paez-Segala et al., 2015) in HEK293T cells. We confirmed the specific integration and functionality of the PCR-tagged MET-mEos4b fusion protein by biochemical methods. Using quantitative super-resolution microscopy, we show that resting MET is largely present as a monomer, whereas in cells treated with the ligands hepatocyte growth factor (HGF) or internalin B (InlB), MET dimers are found. In addition, we performed live-cell single-particle tracking (SPT) experiments of MET-mEos4b and analyzed receptor mobility in untreated cells and upon treatment with HGF.

In summary, we propose PCR tagging as a suitable method for endogenous, stoichiometric, and efficient protein labeling, which in combination with super-resolution microscopy and SPT allows for nanoscopic spatial resolution, quantitative information on protein assemblies, and a native view on protein dynamics.

RESULTS

Endogenous tagging of the MET receptor for single-molecule super-resolution microscopy

A recent study introduced PCR tagging as a simple and time-efficient method for genetic labeling of target proteins (Füller et al., 2020), which makes it a promising labeling tool for quantitative super-resolution microscopy. Using PCR tagging, we generated a stable cell line in which mEos4b was fused C-terminally to the endogenous MET receptor (Figure 1A). We designed two primers to generate a PCR cassette that is specific for the MET gene and transfected HEK293T cells with the PCR cassette and the Cas12a helper plasmid. After selection of CRISPR/Cas12a-tagged cells via puromycin, individual clones were isolated and verified by fluorescence signals. Pronounced fluorescence was observed in 10 of 16 clones tested. These 10 fluorescent clones were divided into five clones with very high fluorescence and five clones with moderate fluorescence after irradiation with 405 nm. A clone with high fluorescence and a clone with moderate fluorescence were randomly selected and further analyzed by two PCRs that amplified DNA sequences at both ends of the inserted region (outside of the homology arms of the PCR cassette) (Figure 1A). DNA fragments of the expected size were found in both PCRs in one clone showing a moderate fluorescence (Figure 1B; MET C6; duplicate), while the other clone (high fluorescence) was positive in only one PCR (data not shown). Sequencing of the purified PCR fragment of MET C6 cells confirmed the correct insertion of mEos4b, hereafter referred to as MET-mEos4b.

Multiple copies of the chromosome in polyploid cells can lead to a mixed population of tagged and untagged receptors, which decreases the labeling efficiency if not all chromosomal sites are targeted. HEK293T cells contain two or more copies of each chromosome (in total 64–70 chromosomes (Stepanenko et al., 2015)), which is still a moderate number compared to other cell lines (e.g., HeLa, 76–80 (Macville et al., 1999)). We determined the labeling efficiency in the MET-mEos4b cell line from a western blot and found a shift of the MET receptor band of about 25–30 kDa for the stable cell line compared to wild-type MET in HEK293T cells (Figure 1C). This

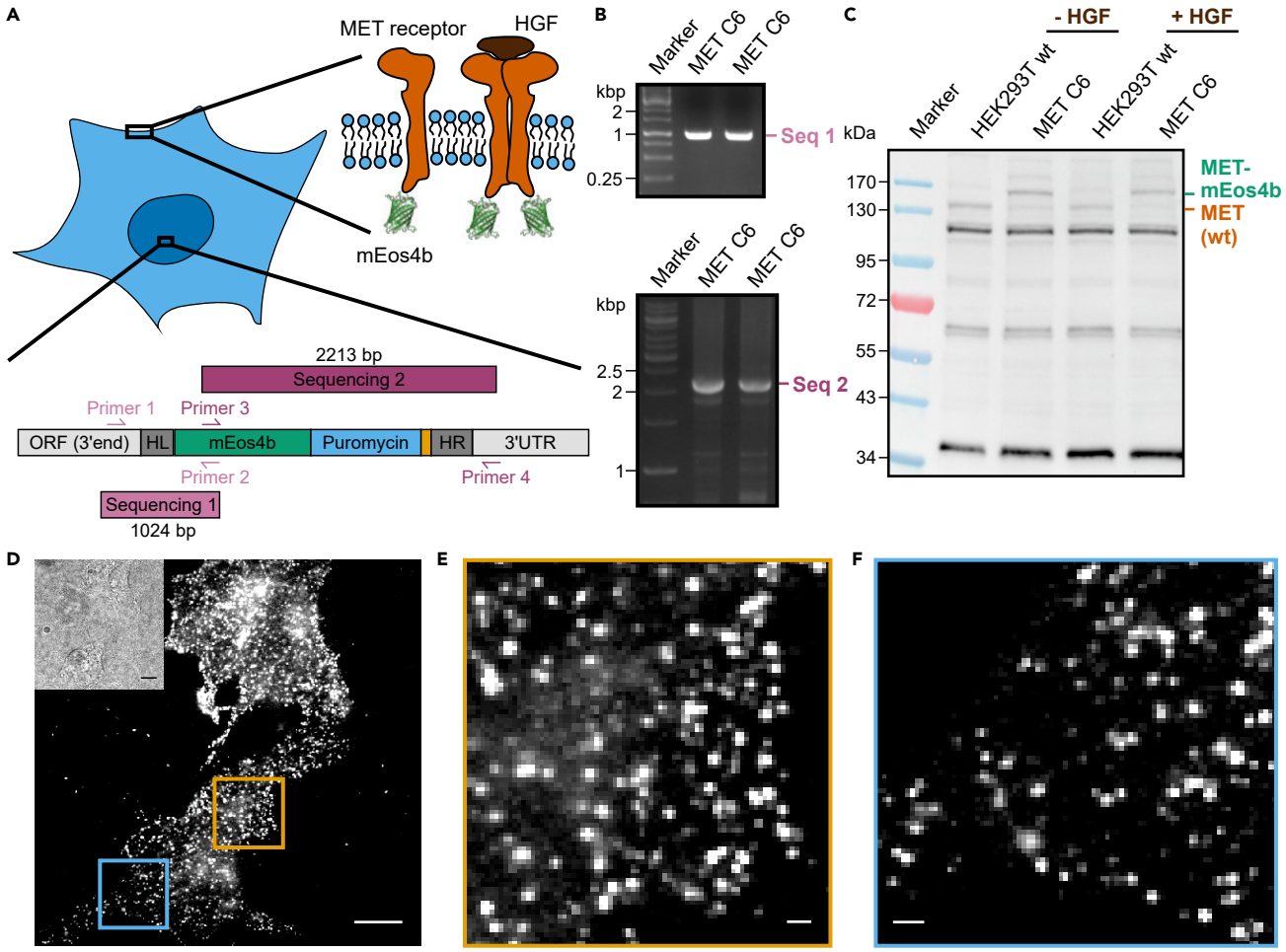

Figure 1. Endogenous tagging of the MET receptor with mEos4b in HEK293T cells

(A) Scheme of the generated MET-mEos4b stable cell line showing both the inserted DNA sequence as well as the expressed fusion protein. The inserted DNA fragment as well as the primers that amplify sequences 1 and 2 and whose PCR product includes the inserted fragment as well as a region outside the homology arms (HL and HR, respectively) of the PCR cassette are shown.

(B) Agarose gel of the amplified PCR products generated with the primers shown in (A). The markers indicate the size of the amplified DNA products.

(C) Western blot with an antibody against the MET receptor in wild-type and PCR-tagged cells with and without the addition of HGF.

(D) Standard deviation image of a PALM movie of MET-mEos4b cells. The brightfield image is shown at the upper left. Scale bar represents 10 μm.

(E and F) Magnified view of the regions highlighted in the standard deviation image shown in (D) of MET-mEos4b cells. Scale bars of 1 μm.

See also Figure S1.

shift in protein size reflects the fusion of the fluorescent protein mEos4b to the MET receptor. In order to determine the fraction of untagged versus tagged receptors in the MET-mEos4b clone, we quantified the band intensities at about 140 kDa and 170 kDa and found that the MET-mEos4b cell line contains approximately 81% mEos4b-tagged MET receptors and 19% of unlabeled MET.

Next, we verified that MET-mEos4b is active by stimulating cells with the physiological ligand of MET, HGF, as well as with a fluorophore-labeled variant of the bacterial ligand InlB, $InlB_{321}$-ATTO 647N, which also targets the MET receptor and was characterized in earlier studies by single-molecule methods (Dietz et al., 2013, 2019; Harwardt et al., 2017). In western blots, MET-mEos4b was phosphorylated upon stimulation with both, HGF and $InlB_{321}$, while untreated cells did not result in phosphorylation of the MET receptor (Figure S1A). Since phosphorylation alone might not necessarily lead to a cellular response (Liang et al., 2018), functional downstream signaling upon stimulation was verified by analyzing the phosphorylation of mitogen-activated protein kinase (Figure S1B). Together, these results demonstrate the native behavior and the same activation pattern of MET-mEos4b compared to wild-type MET receptor.

Upon the verification of efficient labeling and functionality of MET, the next step was to investigate its correct localization at the cell membrane. For that, we performed PALM measurements of HEK293T wild-type cells and the stable cell line expressing MET-mEos4b. While wild-type cells showed only unspecific signal, cells expressing MET-mEos4b showed a clear punctate fluorescence signal at the basal cell membrane with total internal reflection illumination (Figures 1D–1F). We determined the localization precision of MET-mEos4b using a nearest neighbor analysis (Endesfelder et al., 2014) and obtained an average value of 10 ± 3 nm. Furthermore, we addressed the cell-to-cell heterogeneity of MET-mEos4b cells. We determined the number of nanoclusters per μm^2 and found only small variations between single cells (0.63 ± 0.32 cluster/μm^2). In summary, these data demonstrate that we have generated a cell line that expresses fully active MET-mEos4b at an expression level of the wild-type MET receptor.

Changes in oligomerization of endogenous MET after receptor activation

Stoichiometric and efficient labeling is particularly important for quantitative imaging of proteins with microscopy. We were explicitly interested to explore the potential of PCR tagging in quantitative super-resolution microscopy. Quantitative SMLM demands for high-efficient stoichiometric labeling and provides information on protein organization within nanoclusters in cells that is otherwise inaccessible (Krüger et al., 2017; Karathanasis et al., 2020; Möller et al., 2020). These nanoclusters consist of one or more proteins that cannot be resolved as individual units because of a protein packing density within these nanoclusters that is beyond the resolution capabilities of super-resolution PALM. However, the quantitative analysis of fluorescent protein emission kinetics allows to extract the oligomeric state of proteins within these nanoclusters (Dietz and Heilemann, 2019). Here, we used quantitative PALM (qPALM) (Fricke et al., 2015; Hummer et al., 2016; Baldering et al., 2019a) and aimed to determine the oligomeric state of MET-mEos4b before and after ligand stimulation.

In order to determine whether mEos4b is suitable for qPALM analysis, we first imaged single mEos4b immobilized on a glass surface and analyzed the bleaching probability (p-value) from the single-molecule "blinking" statistics (Figures S2A and S2B). We found a p-value of 0.34 ± 0.01, which is similar to the p-value of mEos3.2 (0.32) (Baldering et al., 2019b), thus showing that mEos4b is suitable for qPALM (Figure S2C). Previous measurements have shown that reference proteins such as CD86 and CTLA4 can serve as monomeric and dimeric reference proteins to determine the photophysical parameters directly in cells (Fricke et al., 2015; Baldering et al., 2019b). We generated CD86-mEos4b and CTLA4-mEos4b plasmids, transfected these plasmids into HEK293T cells, recorded PALM images, and performed qPALM analysis. We found a p-value of 0.27 for CD86-mEos4b (Figures S2D and S2E), which is equal to that of CD86-mEos3.2 (Baldering et al., 2019b). Next, we used this p-value to analyze the detection efficiency of mEos4b by fitting the CTLA4-mEos4b histogram with a dimeric fit function (Figures S2F and S2G). We obtained a *q*-value of 0.35, which is slightly lower compared to that of CTLA4-mEos3.2 ($q = 0.39$) (Baldering et al., 2019b). A *q*-value of 0.35 translates into a detection efficiency of 79% (see Equation 1 in Supplemental Information). To additionally include the fraction of unlabeled MET receptors, we multiplied the detection efficiency (0.79) with the labeling efficiency (0.81) and obtain an absolute detection efficiency (0.64) that corrects for all undetected MET receptors. We used these parameters ($p = 0.27$; $d = 0.64$) to analyze the oligomerization of MET-mEos4b in its resting state and found 5% ±1% of MET-mEos4b to be dimeric (Figures 2A and S2H). Upon addition of 1 nM HGF, MET-mEos4b showed a dimeric fraction of 71 ± 3% (Figures 2B and S2I). This shows an explicit shift to dimeric MET in the ligand-stimulated state in agreement with the activation model of MET (Comoglio et al., 2008). In an additional experiment, we treated cells with 5 nM of the bacterial ligand $InlB_{321}$-ATTO 647N (Figure S3A). By analyzing receptor clusters on the membrane, we obtained 63 ± 2% dimers, slightly lower compared to the activation of MET with 1 nM HGF (Figure S3B). Additionally, we analyzed receptors only when co-localizing with $InlB_{321}$-ATTO 647N, assuming that these co-localizations show receptors that are bound to $InlB_{321}$-ATTO 647N. The analysis of co-localized spots showed a slightly increased dimer fraction of 68 ± 4% (Figure S3C). These results confirm the ligand-stimulated dimerization of receptor tyrosine kinases.

Single-particle tracking reveals reduced mobility and immobilization of MET receptors upon ligand stimulation

Receptor mobility was found to respond to ligand binding for various receptor tyrosine kinases (Schlessinger, 2002; Ibach et al., 2015; Harwardt et al., 2020). Therefore, we expected a reduced receptor mobility and an increased fraction of immobile receptors upon stimulation of MET with its physiological ligand HGF or the bacterial ligand $InlB_{321}$. First, we performed live-cell SPT PALM (sptPALM) (Manley et al., 2008) of MET-mEos4b by observing the dynamics of MET receptors. In the resting state, MET-mEos4b was mostly

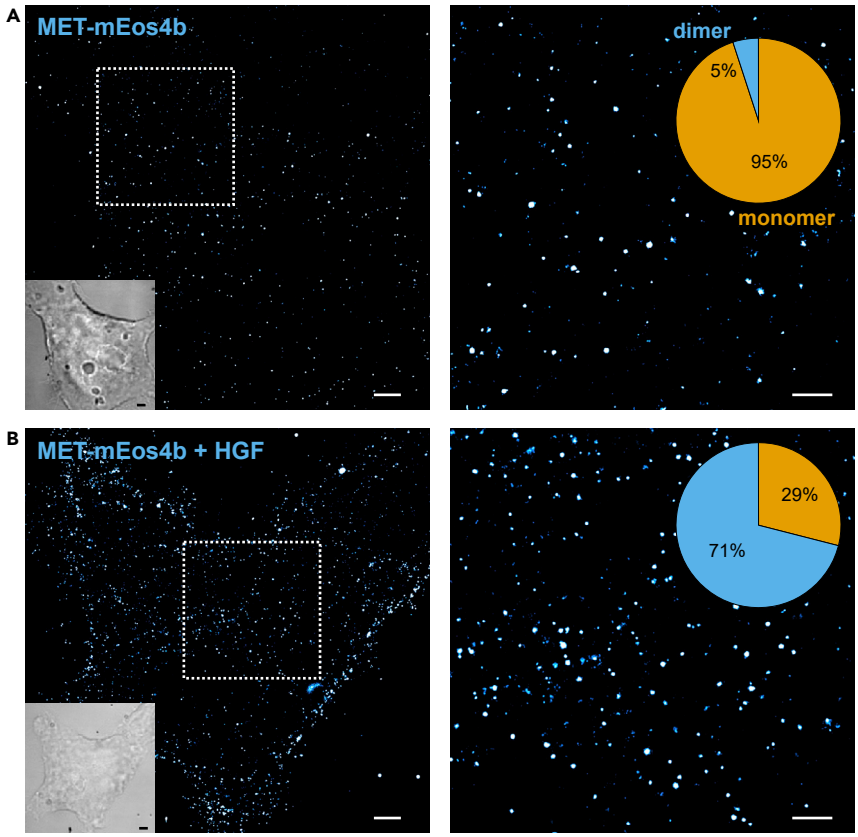

Figure 2. Quantitative PALM analysis of ligand-stimulated and resting MET-mEos4b receptors

qPALM images (left side) of resting (A) and HGF-activated MET-mEos4b cells (B). Zoom-ins of regions marked in the left images are shown (right side) with monomer/dimer ratios depicted as pie charts. Scale bars represent 2 μm and 1 μm. See also Figures S2 and S3.

freely diffusing in the membrane of HEK293T cells; only a small fraction of immobile receptors was observed (Figure 3A). In contrast, HGF-stimulated cells showed a strong decrease in free diffusion (Figure 3B). Considerably, more receptors were immobilized showing small diffusion coefficients. To obtain information on diffusion types, we analyzed the trajectories using a mean square displacement (MSD) analysis (Rossier et al., 2012). In resting cells, the relative frequency of the immobile fraction was 15± 2% (Figure 3C). sptPALM measurements of MET-mEos4b with 1 nM $InlB_{321}$-ATTO 647N approximately doubled the immobile fraction to 27±3%. Stimulation with 1 nM of the physiological ligand HGF showed a large immobile fraction of 72±3%. Additionally, we show that the diffusion coefficients of the confined and free states decrease with the addition of ligands (Figure 3C). These results demonstrate the sensitivity of MET-mEos4b to its natural ligands and prove the ligand-stimulated immobilization of receptors.

Finally, we performed live-cell universal PAINT (uPAINT) (Giannone et al., 2010) measurements of MET-mEos4b treated with $InlB_{321}$-ATTO 647N by detecting the signal of ATTO 647N, as described recently (Rossier et al., 2012; Harwardt et al., 2017). This enabled us to compare the dynamics of labeled $InlB_{321}$ with mEos4b fused to the MET receptor (Figure S4). The MSD analysis of MET-mEos4b showed lower fractions of immobile receptors (27 ±3%) compared to $InlB_{321}$-ATTO 647N (44 ±3%), and diffusion coefficients of $InlB_{321}$-ATTO647N were smaller for confined and free diffusion.

In summary, these results indicate that endogenous tagging by CRISPR/Cas12a in combination with quantitative super-resolution imaging and SPT is a powerful tool to address the molecular organization and dynamics of membrane receptors at an endogenous expression level.

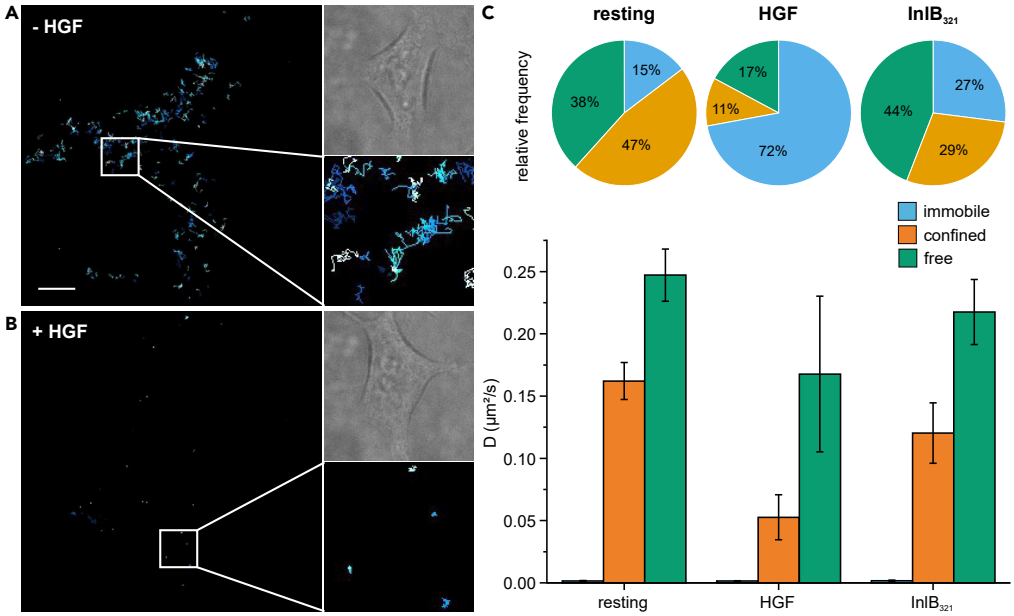

Figure 3. Live-cell single-particle tracking PALM of ligand-stimulated and resting MET-mEos4b

SPT analysis of MET-mEos4b in resting (A) and HGF-stimulated (B) cells. The brightfield image and a zoom-in are shown on the right side. Scale bar represents 5 µm.

(C) MSD-based diffusion type analysis of resting, HGF-stimulated, and $InlB_{321}$-ATTO 647N-stimulated MET-mEos4b cells. Diffusion coefficients with their standard error of the mean (bar diagram) and the respective fractions (pie charts) of the diffusion states: immobile (blue), confined (orange), and free (green) are shown in their respective color. See also Figure S4.

DISCUSSION

The generation of stable cell lines, that express fluorophore-labeled proteins at an endogenous expression level is time intense and often yields poor labeling efficiencies. CRISPR/Cas9 in combination with PALM was used in some studies to label intracellular proteins. The CRISPR/Cas9 method requires (i) a crRNA and tracrRNA expression vector and (ii) cloning of the donor template for homologous insertion of the protein tag. The generation of crRNA expression vectors is usually straightforward, however, requires up to one week for the complete verification of the generated vector. In addition, the synthesis of a donor template by, e.g., Gibson assembly, requires several assemblies to combine all important fragments such as the homologous regions, the tag and an antibiotic resistance (Khan et al., 2017). In comparison, PCR tagging requires less than one day to generate the necessary tools (PCR cassette) for transfection. Since CRISPR/Cas12a is used for PCR tagging, no crRNA expression vector is required as the crRNA is expressed by the PCR cassette itself. Additionally, complicated Gibson assembly reactions are replaced by a simple PCR with primers that can be easily designed. Therefore, PCR tagging enables straightforward and time-efficient gene editing at the C-terminus of proteins of interest (Füller et al., 2020), making it a promising labeling tool for super-resolution microscopy (Figure 4).

We successfully generated a stable cell line expressing MET-mEos4b (Figures 4A–4E). This process was straight forward and time-efficient and will be easily transferable to other targets as previously shown (Füller et al., 2020). We showed the correct insertion of mEos4b into the genome, as well as its homogeneous and endogenous protein expression levels. Füller et al. (2020) reported that occasional off-target integrands seem to result only from spontaneous integrations and that the presence of Cas12a does not promote specific off-target integrands but only on-target integrands (Füller et al., 2020). Since the authors did not observe that such off-target integrations lead to the expression of aberrant fusion proteins, together with our data showing fluorescence emission originating from the plasma membrane but not the cytosol, it is very likely that only the MET receptor effectively expresses mEos4b as a fusion protein.

Further, we verified the activity of the MET-mEos4b fusion protein by western blots. To highlight the various benefits of PCR tagging, we analyzed endogenously tagged MET as transient transfection can

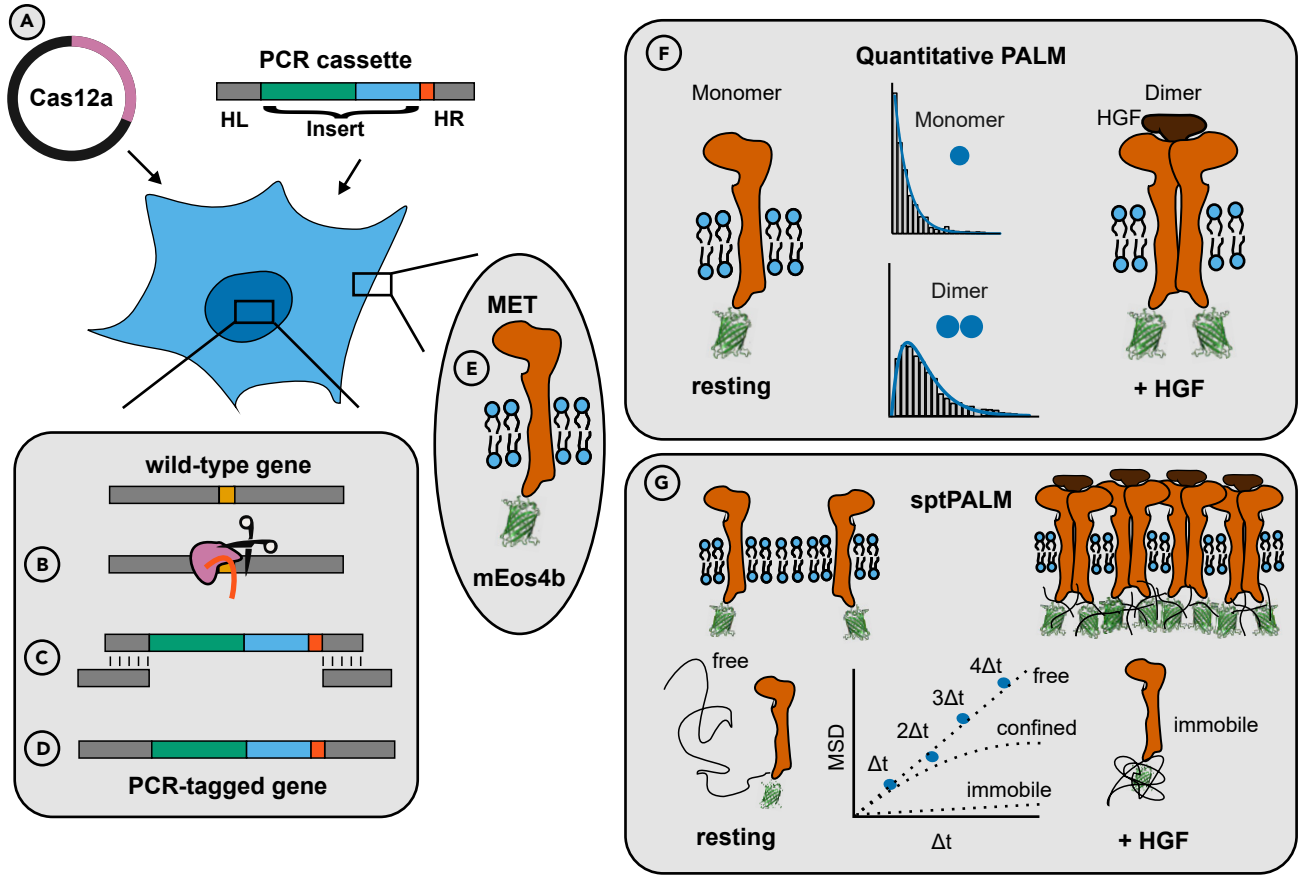

Figure 4. Schematic overview of PCR tagging and possible applications in combination with SMLM

(A) Transfection of HEK293T cells with the Cas12a helper plasmid and the individual PCR cassette.

(B) Cas12a (pink) cuts the DNA at the target site.

(C) The PCR cassette anneals with its homology regions on the genomic DNA and repairs the genomic DNA by homology directed repair (HDR).

(D) Illustration of the PCR-tagged gene.

(E) The protein of interest is expressed as fusion protein with the tag, e.g., a fluorescent protein, here mEos4b (structure of mEos2 shown; PDB:3S05).

(F) qPALM analysis of the PCR-tagged protein of interest reveals its oligomeric state. The MET receptor shows an increased population of dimers in HGF-stimulated cells.

(G) Mobility analysis of the PCR-tagged protein of interest with sptPALM. Schematic illustration of MET receptors shows slowdown and immobilization upon HGF stimulation.

induce artifacts due to non-native expression levels (Lisenbee et al., 2003; Doyon et al., 2011; Gibson et al., 2013). We showed the endogenous expression by analyzing the cluster density (cluster/μm^2) of MET-mEos4b in HEK293T cells. Higher cluster numbers were reported for endogenous MET in HeLa cells in DNA-PAINT measurements (Harwardt et al., 2020). However, taking into account the different mRNA expression levels of MET in HeLa and HEK293T cells (the Human Protein Atlas; www.proteinatlas.org), we expect a lower receptor cluster density for HEK293T cells, which fits to our PALM data and supports an endogenous expression level.

Besides endogenous expression, high labeling efficiency is also important for quantitative analysis. In particular, achieving a high labeling efficiency can be very demanding since the gene of interest can occur on several chromosomes due to multiple sets of chromosomes. PCR tagging allowed us to establish a cell line expressing MET-mEos4b with a protein labeling efficiency of approximately 81%. We assume that our HEK293T cell line contains three copies of chromosome 7 (containing the MET gene) (Stepanenko et al., 2015), where two chromosomes are tagged and transcribed at a higher rate compared to the untagged chromosome (Lo et al., 2003). We achieved this high efficiency through the usage of Cas12a since it has a high specificity *in vivo* (Kleinstiver et al., 2016) and cuts the DNA away from the Cas12a recognition

site. This results in repetitive DNA cuts and thus an increased probability for successful incorporation of the homology template DNA (Zetsche et al., 2015; Moreno-Mateos et al., 2017).

The high tagging efficiency allowed us to quantitatively study the stoichiometry of MET receptor in single signaling complexes. We found monomeric MET receptors in absence of a ligand and strongly increased dimerization in the presence of its natural ligand HGF (Figure 4F). This dimeric shift is in agreement with the generally accepted model of ligand-induced dimerization (Schlessinger, 2002), as well as with recent studies on MET dimerization (Li et al., 2020). For the bacterial ligand $InlB_{321}$, we observed a similar increase in dimerization. In previous single-molecule photobleaching experiments, a lower degree of MET dimerization was observed in HeLa cells (Dietz et al., 2013). In addition to the different cell lines, this difference can be explained by incomplete labeling of receptor dimers with $InlB_{321}$-ATTO 647N, as well as unlabeled $InlB_{321}$. We would therefore like to emphasize the benefit of a high tagging efficiency for quantitative SMLM that is provided by PCR tagging.

We further performed SPT experiments of the tagged MET receptor, which showed ligand-induced reduction in the mobility as well as immobilization of receptors (Figure 4G). The diffusion coefficients of MET-mEos4b in resting and ligand-stimulated conditions are similar to previously published values of endogenous HeLa cells (Harwardt et al., 2017). Both studies show ligand-induced slowdown of MET receptor mobility, which demonstrates the reproducibility of MET dynamics in different cell lines. HGF and $InlB_{321}$ showed differently pronounced effects on MET dynamics, which are consistent with the higher affinity of HGF compared to $InlB_{321}$ (Lokker et al., 1992; Dietz et al., 2013). Additionally, we analyzed the dynamics of MET-mEos4b and labeled $InlB_{321}$ in the same cells, which enabled us to determine the dynamics of total MET receptors and of only stimulated ones. As expected, solely $InlB_{321}$-stimulated receptors showed a higher fraction of immobile receptors. Further, diffusion coefficients of exclusively stimulated receptors were smaller compared with the total number of receptors. Since mEos4b and ATTO 647N are spectrally well separated, this opens the door for two-color SPT by investigating the receptor and its ligand at the same time.

In summary, we demonstrate the simple and time-efficient generation of a PCR-tagged cell line and demonstrate super-resolution imaging and single-protein tracking in live cells (Figure 4). We present endogenous labeling of MET-mEos4b as a proof of principle and confirm biological processes such as ligand-stimulated dimerization and immobilization of receptor tyrosine kinases.

Limitations of the study

This study demonstrates CRISPR/Cas12a-assisted chromosomal labeling of a plasma membrane receptor with a photoswitchable fluorescent protein for quantitative single-molecule super-resolution microscopy. The protocol for CRISPR/Cas12a-assisted chromosomal labeling used in this work allows C-terminal labeling of proteins with fluorescent reporters. Quantitative PALM operates best for low-number oligomers and in total internal reflection fluorescence (TIRF) imaging mode.

Resource availability

Lead contact

Further information and requests for resources and reagents should be directed to and will be fulfilled by the Lead Contact, Prof. Dr. Mike Heilemann, heileman@chemie.uni-frankfurt.de.

Materials availability

Additional information including reasonable requests for materials such as plasmids should be directed to and will be conducted by the Lead Contact.

Data and code availability

The data included in this study are available from the Lead Contact on reasonable request.

METHODS

All methods can be found in the accompanying Transparent Methods supplemental file.

SUPPLEMENTAL INFORMATION

Supplemental Information can be found online at https://doi.org/10.1016/j.isci.2020.101895.

ACKNOWLEDGMENTS

We are grateful to the Volkswagen Foundation (grant 91067-9), LOEWE (FCI), and the Deutsche Forschungsgemeinschaft (grant SFB807) for financial support. M.K. acknowledges support from the Deutsche Forschungsgemeinschaft (grant KN498/12-1). We thank Daniel Haβe and Hartmut H. Niemann for providing labeled $InlB_{321}$ and Robert Tampé for providing access to the chemiluminescence reader. Finally, we thank Sebastian Malkusch for helpful discussions.

AUTHOR CONTRIBUTIONS

Conceptualization, T.N.B., M.S.D., and M.H.; Methodology, M.K., M.M, T.N.B, M.S.D., and M.H; Investigation, T.N.B., C.K., M.-L.I.E.H., and P.F.; Writing – Original Draft, T.N.B., M.S.D., and M.H.; Writing – Review & Editing, C.K., M.-L.I.E.H., P.F., J.V.R., M.M., and M.K.; Funding Acquisition, M.H.; Resources, M.K. and M.M.; Supervision, M.H. and M.S.D.

DECLARATION OF INTERESTS

The authors declare no competing interests.

Received: August 14, 2020
Revised: November 12, 2020
Accepted: December 2, 2020
Published: January 22, 2021

REFERENCES

Baldering, T.N., Bullerjahn, J.T., Hummer, G., Heilemann, M., and Malkusch, S. (2019a). Molecule counts in complex oligomers with single-molecule localization microscopy. J. Phys. D Appl. Phys. *52*, 474002.

Baldering, T.N., Dietz, M.S., Gatterdam, K., Karathanasis, C., Wieneke, R., Tampé, R., and Heilemann, M. (2019b). Synthetic and genetic dimers as quantification ruler for single-molecule counting with PALM. Mol. Biol. Cell *30*, 1369–1376.

Betzig, E., Patterson, G.H., Sougrat, R., Lindwasser, O.W., Olenych, S., Bonifacino, J.S., Davidson, M.W., Lippincott-Schwartz, J., and Hess, H.F. (2006). Imaging intracellular fluorescent proteins at nanometer resolution. Science *313*, 1642–1645.

Cho, W.-K., Jayanth, N., Mullen, S., Tan, T.H., Jung, Y.J., and Cissé, I.I. (2016). Super-resolution imaging of fluorescently labeled, endogenous RNA Polymerase II in living cells with CRISPR/Cas9-mediated gene editing. Sci. Rep. *6*, 35949.

Comoglio, P.M., Giordano, S., and Trusolino, L. (2008). Drug development of MET inhibitors. Targeting oncogene addiction and expedience. Nat. Rev. Drug Discov. *7*, 504–516.

Deltcheva, E., Chylinski, K., Sharma, C.M., Gonzales, K., Chao, Y., Pirzada, Z.A., Eckert, M.R., Vogel, J., and Charpentier, E. (2011). CRISPR RNA maturation by trans-encoded small RNA and host factor RNase III. Nature *471*, 602–607.

Dietz, M.S., Haße, D., Ferraris, D.M., Göhler, A., Niemann, H.H., and Heilemann, M. (2013). Single-molecule photobleaching reveals increased MET receptor dimerization upon ligand binding in intact cells. BMC Biophys. *6*, 6.

Dietz, M.S., and Heilemann, M. (2019). Optical super-resolution microscopy unravels the molecular composition of functional protein complexes. Nanoscale *11*, 17981–17991.

Dietz, M.S., Wehrheim, S.S., Harwardt, M.-L.I.E., Niemann, H.H., and Heilemann, M. (2019). Competitive binding study revealing the influence of fluorophore labels on biomolecular interactions. Nano Lett. *19*, 8245–8249.

Doyon, J.B., Zeitler, B., Cheng, J., Cheng, A.T., Cherone, J.M., Santiago, Y., Lee, A.H., Vo, T.D., Doyon, Y., Miller, J.C., et al. (2011). Rapid and efficient clathrin-mediated endocytosis revealed in genome-edited mammalian cells. Nat. Cell Biol. *13*, 331–337.

Endesfelder, U., Malkusch, S., Fricke, F., and Heilemann, M. (2014). A simple method to estimate the average localization precision of a single-molecule localization microscopy experiment. Histochem. Cell Biol. *141*, 629–638.

Fricke, F., Beaudouin, J., Eils, R., and Heilemann, M. (2015). One, two or three? Probing the stoichiometry of membrane proteins by single-molecule localization microscopy. Sci. Rep. *5*, 14072.

Füller, J., Herbst, K., Meurer, M., Gubicza, K., Kurtulmus, B., Knopf, J.D., Kirrmaier, D., Buchmuller, B.C., Pereira, G., Lemberg, M.K., and Knop, M. (2020). CRISPR-Cas12a-assisted PCR tagging of mammalian genes. J. Cell Biol. *219*, e201910210.

Giannone, G., Hosy, E., Levet, F., Constals, A., Schulze, K., Sobolevsky, A.I., Rosconi, M.P., Gouaux, E., Tampé, R., Choquet, D., and Cognet, L. (2010). Dynamic superresolution imaging of endogenous proteins on living cells at ultra-high density. Biophys. J. *99*, 1303–1310.

Gibson, T.J., Seiler, M., and Veitia, R.A. (2013). The transience of transient overexpression. Nat. Methods *10*, 715–721.

Hansen, A.S., Pustova, I., Cattoglio, C., Tjian, R., and Darzacq, X. (2017). CTCF and cohesin regulate chromatin loop stability with distinct dynamics. Elife *6*, e25776.

Harwardt, M.-L.I.E., Schröder, M.S., Li, Y., Malkusch, S., Freund, P., Gupta, S., Janjic, N., Strauss, S., Jungmann, R., Dietz, M.S., and Heilemann, M. (2020). Single-molecule super-resolution microscopy reveals heteromeric complexes of MET and EGFR upon ligand activation. Int. J. Mol. Sci. *21*, 2803.

Harwardt, M.-L.I.E., Young, P., Bleymüller, W.M., Meyer, T., Karathanasis, C., Niemann, H.H., Heilemann, M., and Dietz, M.S. (2017). Membrane dynamics of resting and internalin B-bound MET receptor tyrosine kinase studied by single-molecule tracking. FEBS Open Bio *7*, 1422–1440.

Hummer, G., Fricke, F., and Heilemann, M. (2016). Model-independent counting of molecules in single-molecule localization microscopy. Mol. Biol. Cell *27*, 3637–3644.

Ibach, J., Radon, Y., Gelléri, M., Sonntag, M.H., Brunsveld, L., Bastiaens, P.I.H., and Verveer, P.J. (2015). Single particle tracking reveals that EGFR signaling activity is amplified in clathrin-coated pits. PLoS One *10*, e0143162.

Karathanasis, C., Medler, J., Fricke, F., Smith, S., Malkusch, S., Widera, D., Fulda, S., Wajant, H., van Wijk, S.J.L., Dikic, I., and Heilemann, M. (2020). Single-molecule imaging reveals the oligomeric state of functional TNFα-induced plasma membrane TNFR1 clusters in cells. Sci. Signal. *13*, eaax5647.

Khan, A.O., Simms, V.A., Pike, J.A., Thomas, S.G., and Morgan, N.V. (2017). CRISPR-Cas9 mediated labelling allows for single molecule imaging and resolution. Sci. Rep. *7*, 8450.

Khan, A.O., White, C.W., Pike, J.A., Yule, J., Slater, A., Hill, S.J., Poulter, N.S., Thomas, S.G., and Morgan, N.V. (2019). Optimised insert design for improved single-molecule imaging and quantification through CRISPR-Cas9 mediated knock-in. Sci. Rep. *9*, 14219.

Kim, H.K., Song, M., Lee, J., Menon, A.V., Jung, S., Kang, Y.-M., Choi, J.W., Woo, E., Koh, H.C., Nam, J.-W., and Kim, H. (2017). In vivo high-throughput profiling of CRISPR-Cpf1 activity. Nat. Methods *14*, 153–159.

Kleinstiver, B.P., Tsai, S.Q., Prew, M.S., Nguyen, N.T., Welch, M.M., Lopez, J.M., McCaw, Z.R., Aryee, M.J., and Joung, J.K. (2016). Genome-wide specificities of CRISPR-Cas Cpf1 nucleases in human cells. Nat. Biotechnol. *34*, 869–874.

Krüger, C.L., Zeuner, M.-T., Cottrell, G.S., Widera, D., and Heilemann, M. (2017). Quantitative single-molecule imaging of TLR4 reveals ligand-specific receptor dimerization. Sci. Signal. *10*, eaan1308.

Le Cong, Ran, F.A., Cox, D., Lin, S., Barretto, R., Habib, N., Hsu, P.D., Wu, X., Jiang, W., Marraffini, L.A., and Zhang, F. (2013). Multiplex genome engineering using CRISPR/Cas systems. Science *339*, 819–823.

Li, Y., Zhang, X., Pan, W., Li, N., and Tang, B. (2020). A Nongenetic proximity-induced FRET strategy based on DNA tetrahedron for visualizing the receptor dimerization. Anal. Chem. *92*, 11921–11926.

Liang, S.I., van Lengerich, B., Eichel, K., Cha, M., Patterson, D.M., Yoon, T.-Y., Zastrow, M.von, Jura, N., and Gartner, Z.J. (2018). Phosphorylated EGFR dimers are not sufficient to activate ras. Cell Rep. *22*, 2593–2600.

Lisenbee, C.S., Karnik, S.K., and Trelease, R.N. (2003). Overexpression and mislocalization of a tail-anchored GFP redefines the identity of peroxisomal ER. Traffic *4*, 491–501.

Lo, H.S., Wang, Z., Hu, Y., Yang, H.H., Gere, S., Buetow, K.H., and Lee, M.P. (2003). Allelic variation in gene expression is common in the human genome. Genome Res. *13*, 1855–1862.

Lokker, N.A., Mark, M.R., Luis, E.A., Bennett, G.L., Robbins, K.A., Baker, J.B., and Godowski, P.J. (1992). Structure-function analysis of hepatocyte growth factor. Identification of variants that lack mitogenic activity yet retain high affinity receptor binding. EMBO J. *11*, 2503–2510.

Macville, M., Schröck, E., Padilla-Nash, H., Keck, C., Ghadimi, B.M., Zimonjic, D., Popescu, N., and Ried, T. (1999). Comprehensive and definitive molecular cytogenetic characterization of HeLa cells by spectral karyotyping. Cancer Res. *59*, 141–150.

Manley, S., Gillette, J.M., Patterson, G.H., Shroff, H., Hess, H.F., Betzig, E., and Lippincott-Schwartz, J. (2008). High-density mapping of single-molecule trajectories with photoactivated localization microscopy. Nat. Methods *5*, 155–157.

Möller, J., Isbilir, A., Sungkaworn, T., Osberg, B., Karathanasis, C., Sunkara, V., Grushevskyi, E.O., Bock, A., Annibale, P., Heilemann, M., et al. (2020). Single-molecule analysis reveals agonist-specific dimer formation of μ-opioid receptors. Nat. Chem. Biol. *16*, 946–954.

Moreno-Mateos, M.A., Fernandez, J.P., Rouet, R., Vejnar, C.E., Lane, M.A., Mis, E., Khokha, M.K., Doudna, J.A., and Giraldez, A.J. (2017). CRISPR-Cpf1 mediates efficient homology-directed repair and temperature-controlled genome editing. Nat. Commun. *8*, 2024.

Paez-Segala, M.G., Sun, M.G., Shtengel, G., Viswanathan, S., Baird, M.A., Macklin, J.J., Patel, R., Allen, J.R., Howe, E.S., Piszczek, G., et al. (2015). Fixation-resistant photoactivatable fluorescent proteins for CLEM. Nat. Methods *12*, 215–218.

Ran, F.A., Hsu, P.D., Wright, J., Agarwala, V., Scott, D.A., and Zhang, F. (2013). Genome engineering using the CRISPR-Cas9 system. Nat. Protoc. *8*, 2281–2308.

Ratz, M., Testa, I., Hell, S.W., and Jakobs, S. (2015). CRISPR/Cas9-mediated endogenous protein tagging for Resolft super-resolution microscopy of living human cells. Sci. Rep. *5*, 9592.

Rossier, O., Octeau, V., Sibarita, J.-B., Leduc, C., Tessier, B., Nair, D., Gatterdam, V., Destaing, O., Albigès-Rizo, C., Tampé, R., et al. (2012). Integrins β1 and β3 exhibit distinct dynamic nanoscale organizations inside focal adhesions. Nat. Cell Biol. *14*, 1057–1067.

Sauer, M., and Heilemann, M. (2017). Single-molecule localization microscopy in eukaryotes. Chem. Rev. *117*, 7478–7509.

Schermelleh, L., Ferrand, A., Huser, T., Eggeling, C., Sauer, M., Biehlmaier, O., and Drummen, G.P.C. (2019). Super-resolution microscopy demystified. Nat. Cell Biol. *21*, 72–84.

Schlessinger, J. (2002). Ligand-induced, receptor-mediated dimerization and activation of EGF receptor. Cell *110*, 669–672.

Stepanenko, A., Andreieva, S., Korets, K., Mykytenko, D., Huleyuk, N., Vassetzky, Y., and Kavsan, V. (2015). Step-wise and punctuated genome evolution drive phenotype changes of tumor cells. Mutat. Res. *771*, 56–69.

Whelan, D.R., and Bell, T.D.M. (2015). Image artifacts in single molecule localization microscopy. Why optimization of sample preparation protocols matters. Sci. Rep. *5*, 7924.

Yamamoto, Y., and Gerbi, S.A. (2018). Making ends meet. Targeted integration of DNA fragments by genome editing. Chromosoma *127*, 405–420.

Zetsche, B., Gootenberg, J.S., Abudayyeh, O.O., Slaymaker, I.M., Makarova, K.S., Essletzbichler, P., Volz, S.E., Joung, J., van der Oost, J., Regev, A., et al. (2015). Cpf1 is a single RNA-guided endonuclease of a class 2 CRISPR-Cas system. Cell *163*, 759–771.

iScience, Volume *24*

Supplemental Information

CRISPR/Cas12a-mediated labeling of MET receptor enables quantitative single-molecule imaging of endogenous protein organization and dynamics

Tim N. Baldering, Christos Karathanasis, Marie-Lena I.E. Harwardt, Petra Freund, Matthias Meurer, Johanna V. Rahm, Michael Knop, Marina S. Dietz, and Mike Heilemann

Supplemental Information

Supplemental Figures

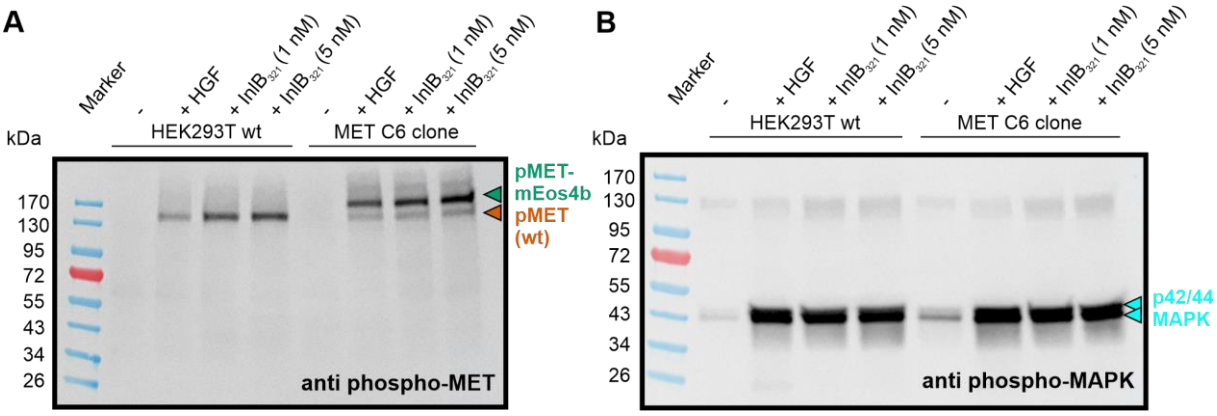

Figure S1. Western blots of ligand-stimulated and resting MET-mEos4b cells. Related to Figure 1. (A) Western blot with an antibody against phospho-MET. Wild-type and MET-mEos4b cells (MET C6) were analyzed under resting conditions as well as upon HGF and $InlB_{321}$-ATTO 647N stimulation. **(B)** Western blot with an antibody against phosphorylated mitogen-activated protein kinase (MAPK) in wild-type (wt) and MET-mEos4b cells (MET C6).

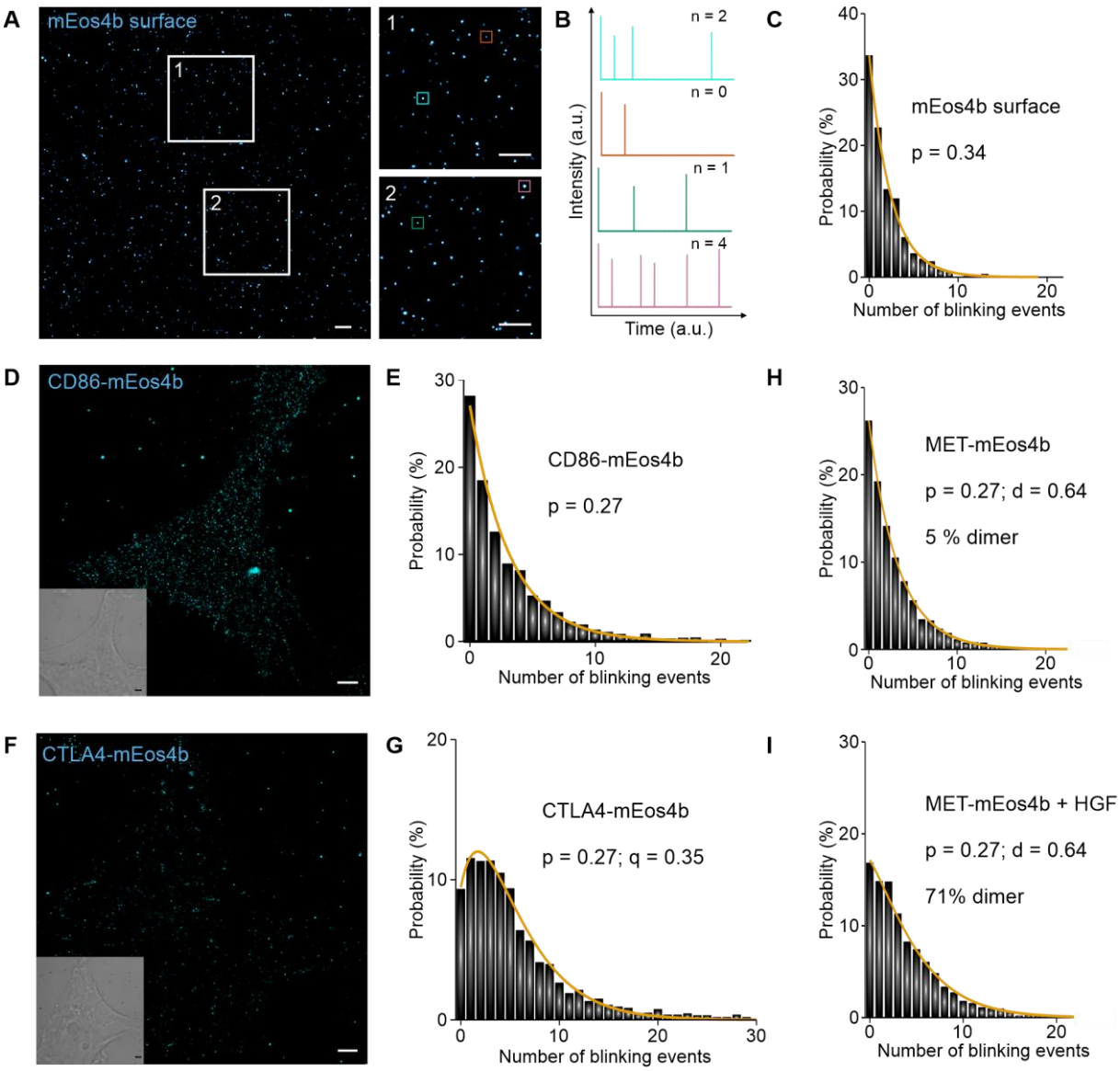

Figure S2. qPALM analysis of single mEos4b molecules as well as resting and HGF-stimulated MET-mEos4b. Related to Figure 2. (A) PALM image of mEos4b on a poly-L-lysine surface with two zoom-ins. Scale bars 2 µm, zoom-ins 1 µm. **(B)** Schematic intensity time traces showing the number of blinking events (n) of single mEos4b molecules. **(C)** Relative frequencies of the number of blinking events of mEos4b molecules (576 clusters). **(D)** PALM image of CD86-mEos4b transfected HEK293T cells. Scale bar is 2 µm. **(E)** Relative frequencies of number of blinking events of CD86-mEos4b molecules (2885 clusters). **(F)** PALM image of CTLA4-mEos4b transfected HEK293T cells. Scale bar is 2 µm. **(G)** Relative frequencies of number of blinking events of CTLA4-mEos4b molecules (2277 clusters). **(H, I)** Relative frequencies of number of blinking events of resting MET-mEos4b (H, 2432 clusters), and HGF-stimulated MET-mEos4b in HEK293T cells (I, 2196 clusters).

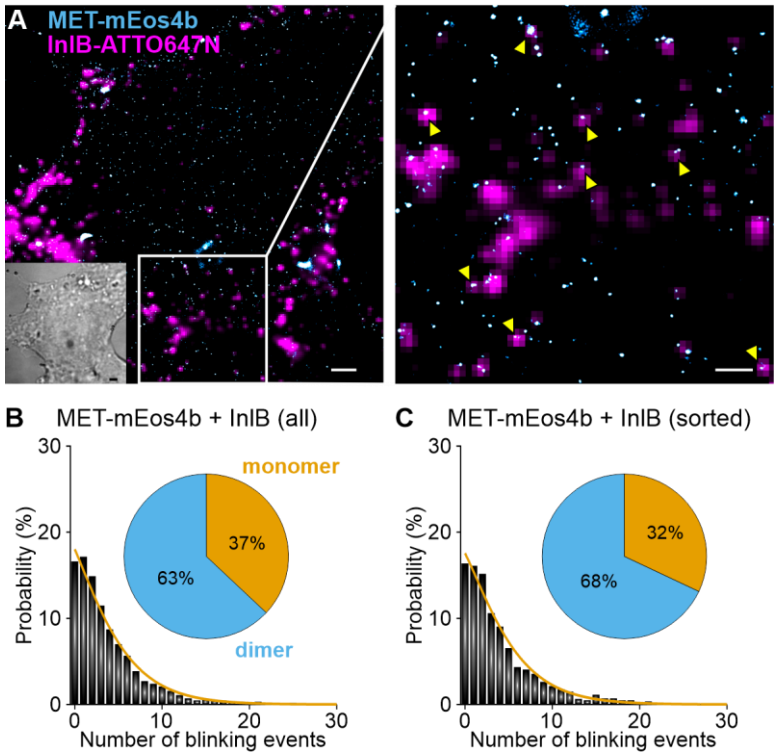

Figure S3. qPALM analysis of InlB$_{321}$-ATTO 647N-stimulated MET-mEos4b cells. Related to Figure 2. (A) qPALM image of MET-mEos4b (cyan) and InlB$_{321}$-ATTO 647N (purple). The brightfield image is shown at the left bottom side. A zoom-in shows the co-localization of MET-mEos4b with InlB$_{321}$-ATTO 647N (yellow arrows). Scale bars 2 µm, zoom-in 1 µm. **(B,C)** Histograms of the relative frequency of blinking events of InlB$_{321}$-ATTO 647N-stimulated MET-mEos4b (B, 3963 clusters) and solely co-localized clusters of MET-mEos4b with InlB$_{321}$-ATTO 647N (C, 1407 clusters).

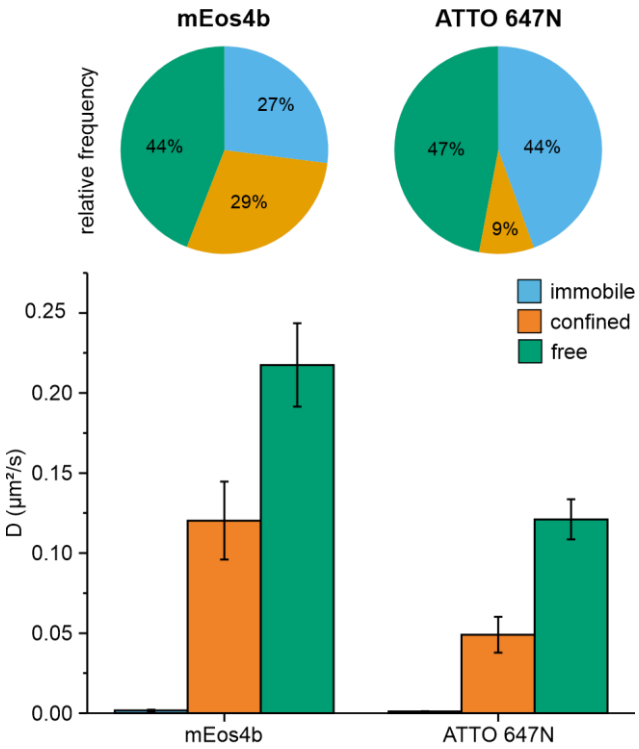

Figure S4. Comparison of live-cell single-particle tracking of MET-mEos4b and InlB$_{321}$-ATTO 647N. Related to Figure 3. MSD analysis of MET-mEos4b (sptPALM) and InlB$_{321}$-ATTO 647N (uPAINT). Diffusion coefficients with their standard error of the mean (bar diagram) and the respective fractions (pie charts) of the diffusion states: immobile (blue); confined (orange), and free (green) are shown in their respective color.

Transparent Methods

Cloning of plasmids

The DNA sequence of mEos4b (pMaCTag-P17, Addgene, plasmid number: #120028) was amplified by PCR (Bio-Rad C1000 Touch™ Thermal Cycler, Bio-Rad laboratories, Hercules, CA, USA) with specific primers (Table 1) and used for cloning into the pRsetA vector for protein expression and purification. The DNA sequence of mEos3.2 (Baldering et al., 2019b) was replaced by mEos4b with standard restriction enzyme cloning and the generated plasmid was verified by DNA sequencing. CD86-mEos4b and CTLA4-mEos4b plasmids were generated in Hot Fusion reactions. PCR fragments were generated with primers (Table 1) containing a 30 base pair overlap, were purified and used in Hot Fusion reactions with 40 ng vector and 200 ng insert in 2x Hot Fusion buffer (0.2 M TRIS HCl pH 7.5, 20 mM $MgCl_2$, 0.4 mM dNTPs, 20 mM DTT, 10% PEG-8000, 0.0075 u/µL T5 exonuclease, and 0.05 u/µL Phusion DNA Polymerase). The Hot Fusion mix was incubated for 1 hour at 50°C, then ramped down to 20°C in 5 minutes (0.1°C per second), and held at 10°C. 3 µL of the Hot Fusion reaction were used for electroporation of *E.coli* Top10 cells. Positive clones were verified by sequencing.

Table S1: List of primers for cloning the plasmids: pRsetA-mEos4b, pirespuro2-CD86-mEos4b and pirespuro2-CTLA4-mEos4b. Related to Figure 2.

Plasmid	Primer name	DNA sequence
mEos4b	mEos4b_fw	GGA GGATCC gtgagtgcgattaagccagacatg
mEos4b	mEos4b_rev	GGA GAATTC tcatcgtctggcattgtcaggc
CD86/CTLA4-mEos4b	Hot_mEos4b_fw	gctgcgctgctggcaaccccggtcgctact gtgagtgcgattaagccagacatgaggatc
CD86/CTLA4-mEos4b	Hot_mEos4b_rev	cacactggatcagttatctatgcggccgct tcatcgtctggcattgtcaggcaatccaga
CD86/CTLA4-mEos4b	Hot_vector_fw	tctggattgcctgacaatgccagacgatga agcggccgcatagataactgatccagtgtg
CD86/CTLA4-mEos4b	Hot_vector_rev	gatcctcatgtctggcttaatcgcactcac agtagcgaccggggttgccagcagcgcagc

Expression and purification of mEos4b

The pRSET vector containing the mEos4b sequence was electroporated (BTX Harvard Apparatus, Gemini System, Thermo Fisher Scientific, MA, USA) into *E.coli* BL21-DE3 cells. Single colonies were picked from a fresh agar plate of electroporated cells and cultivated in 10 mL LB medium (Roth, Karlsruhe, Germany) with the appropriate antibiotic. After about 16 h, 400 mL LB medium was inoculated with 10 mL of the pre-culture and incubated at 37 °C, 200 rpm until the cells reached an OD_{600} (Nanophotometer, IMPLEN, Munich, Germany) of about 0.4. Then, 1 mM isopropyl-ß-D-thiogalactopyranosid (IPTG, Cayman chemical company, MI, USA) was added to induce protein expression for about 16 h at 20 °C, 200 rpm. Then cells were harvested by centrifugation at 4,000 x g for 10 min (Megafuge 1.0, Heraeus, Hanau, Germany). The cell pellet was lysed in 3 mL of lysis buffer (50 mM NaH_2PO_4 (Sigma-Aldrich, MO, USA), 300 mM NaCl (Sigma-Aldrich), 10 mM imidazole (Sigma-Aldrich)) with 1 mM lysozyme (Sigma-Aldrich), a cOmplete Mini EDTA-free protease inhibitor tablet (Roche, Basel, Switzerland) and by 4 x 1 min cycles of sonification (Sonifier 250, Branson Ultrasonics, CT, USA). After lysis, the cell solution was centrifuged two times at 16,900 x g for 15 min (Centrifuge 5418 R, Eppendorf, Hamburg, Germany) and the supernatant was applied onto an equilibrated Ni-NTA column (Qiagen, Venlo, Netherlands). The column was washed with lysis buffer containing 20 mM imidazole and the protein was eluted with lysis buffer containing 250 mM imidazole. Subsequently, the buffer was exchanged to phosphate buffered saline (1xDPBS, Gibco by Thermo Fisher Scientific) by a size-exclusion column. A SDS-PAGE (4-20% gradient SDS gels, BioRad Laboratories, Hercules, USA) analysis verified the correct size of the protein.

Generation of the PCR cassette for endogenous tagging of MET with mEos4b

As a first step of PCR tagging, the PCR cassette was generated (Füller et al., 2020). Primers M1 and M2 (see below) were designed, and a PCR (Bio-Rad C1000 Touch™ Thermal Cycler) was performed with a template plasmid carrying the mEos4b sequence (pMaCTag-P17, Addgene, plasmid number: #120028) (see also: www.PCR-tagging.com). The PCR cassette was purified with a PCR purification kit (Thermo Fisher Scientific GmbH) and further used to transfect HEK293T cells.

Primer M1:
T*G*T*G*T*CGCTCCGTATCCTTCTCTGTTGTCATCAGAAGATAACGCTGATGATGAGGTGGACAC
ACGACCAGCCTCCTTCTGGGAGACATCATCAGGTGGAGGAGGTAGTG

Primer M2:
C*A*G*T*G*AAAAAACCATTGGACAAAGTGTGGACTGTTGCTTTGACATAGTACTAGCAAAAAAAAC
TAGCACTATGATGTCTCCATCTACACTTAGTAGAAATTAGCTAGCTGCATCGGTACC

Transfection of HEK293T cells and generation of stable CRISPR/Cas12a cell lines
HEK293T cells were cultivated in Dulbecco's modified Eagle medium (DMEM) (Gibco, LifeTechnologies) supplemented with 1% GlutaMAX (Gibco, Life Technologies) and 10% fetal bovine serum (Gibco, Life Technologies) in an CO_2 incubator (Model C 150; Binder GmbH, Tuttlingen, Germany) at 37 °C, 5% CO_2 and seeded on 24-well plates (Greiner Bio-One international GmbH, Kremsmünster, Austria) at a density of $4 \cdot 10^4$ cells/well. After one day, co-transfection with the PCR cassette (500 ng/well in 24 well plate) and the appropriate Cas12a expression plasmid (pY230; Addgene, plasmid number: #89355, 500 ng/well in 24 well plate)) was performed with Lipofectamine 3000 (Thermo Fisher Scientific GmbH) (Füller et al., 2020). After approximately 72 h, the cells were transferred into 6-well plates (Greiner Bio-One international GmbH) containing 1.5 µg/mL puromycin (Sigma-Aldrich). The cells were cultivated in medium containing puromycin for approximately 1-2 weeks to reach a density that was suitable for transferring the cells into a t75 flask (Greiner Bio-One international GmbH). Single clones were then selected using a 96-well plate (Thermo Fisher Scientific) containing 1 cell/well. After an additional week, cells from single wells, containing enough cells from solely one clone, were transferred into 1 well per 24 well-plate and cultivated to have enough cells for genome isolation, western blotting, and analysis through fluorescence microscopy.

Genome isolation and analysis of single clones
Genome isolation was performed with approximately $1 \cdot 10^6$ cells by using the Genomic DNA Purification Kit (Thermo Fisher Scientific GmbH). After genome isolation, a PCR was performed with primers annealing in- and outside of the PCR cassette. Fragments were purified and sent to Eurofins genomics for DNA sequence analysis.

Western blot of single clones
Individual clones were seeded on 10 cm dishes at a density of about $1 \cdot 10^6$ cells per dish. After 2.5 days, cell medium was changed to serum-free medium for approximately 12-16 h. Cells were stimulated with 1 nM human HGF (PeproTech GmbH, Hamburg, Germany) and 1 or 5 nM $InlB_{321}$-ATTO 647N for 10 minutes at 37 °C and then washed with PBS once prior to harvesting the cells with 200 µL of cell lysis buffer (50 mM Tris (Sigma-Aldrich), 150 mM NaCl (Sigma-Aldrich), 1% Triton X-100 (Sigma-Aldrich), 1 mM Na_3VO_4 (Sigma-Aldrich), 1mM EDTA (Sigma-Aldrich), 1mM NaF (Sigma-Aldrich), and one-fourth of a cOmplete Mini EDTA-free protease inhibitor tablet (Roche)). After the cells were incubated in a temperature shaker (Thermo-Shaker, Universal Labortechnik GmbH & Co. KG, Leipzig, Germany) at 750 rpm; 4 °C for 5 min, cells were centrifuged at 12,000 x g; 4 °C for 20 min (Centrifuge 5418 R, Eppendorf). The supernatant was collected and supplemented with 5x SDS-loading dye (250 mM Tris-HCl (pH 6.8), 8% (w/v) SDS (Sigma-Aldrich), 0.1% bromphenol blue (Sigma-Aldrich), 40% (v/v) glycerol (Roth)) and a final concentration of 100 mM dithiothreitol (DTT, Sigma-Aldrich). SDS-PAGE was performed with 4-20% gradient SDS gels (BioRad Laboratories) at 200 V for 30-90 min. Gels were blotted with the iBlot Gel Transfer System (Invitrogen, Thermo Fisher Scientific) as described by the manufacturer. After blotting, membranes were transferred into 50 mL tubes and 5% (w/v) nonfat dry milk (Cell Signaling Technology, MA, USA) in Tris-buffered saline containing 0.1% Tween-20 (TBST) was added for 1 h at ambient temperature. The membranes were washed three times with 10 mL TBST and incubated with primary antibody (MET antibody, #4560; phospho-MET antibody (tyr1234/1235), #3077; phospho-MAPK antibody, #9101S; Cell SignalingTechnology, MA, USA, 1:1000) at 4 °C over night. After three additional washing steps with 10 mL TBST, the secondary HRP-tagged antibody (goat anti-rabbit IgG, Jackson ImmunoResearch, PA, USA, 1:20,000) was added for 3 h at ambient temperature. Then, the membrane was washed three times with 10 mL TBST and once with 10 mL TBS for 5-15 min at ambient temperature. Finally, chemiluminescence detection at a Fusion FX Edge imager (Vilber Lourmat, Collégien, France) was performed by using 1 mL of SuperSignal West Femto Maximum Sensitivity Substrate solution (Thermo Fisher Scientific). Western blot bands were analyzed with Fiji

(Schindelin et al., 2012). The integral of the intensity of individual bands was determined, which allowed the fraction of labeled MET receptor to be estimated.

Preparation of functionalized surfaces for SPT and qPALM

Before sample preparation, the cover glass passivation and functionalization was performed (Baldering et al., 2019b). 25 mm round glass coverslips (VWR International, Radnor, USA) or square cover glasses (35 × 64 mm, # 1.5, Thermo Fisher Scientific) were sonicated in 2-propanol (VWR Chemicals) for 20 min, plasmacleaned with nitrogen or oxygen for 15 min (Diener Electronic GmbH, Ebhausen, Germany) and covered with 100 µg/mL of poly-L-lysine (Sigma-Aldrich) or 0.8 mg/mL PLL-PEG-RGD (self-made, for details see (Harwardt et al., 2020)) for 2 h. After washing with H_2O, cover glasses were dried with nitrogen and used immediately or stored under argon gas at -20 °C.

Sample preparation of mEos4b and MET-mEos4b for (q)PALM imaging

The purified mEos4b protein was transferred on a poly-L-lysine coated cover glass (35 × 64 mm, #1.5, Thermo Fisher Scientific) using 8-well flexiPERMs (Sarstedt) at a concentration suitable for PALM imaging (about 1 nM) and incubated for 30 min at ambient temperature. After that, the chambers were washed three times with sterile-filtered PBS and PALM movies were recorded in sterile-filtered PBS.

200 ng plasmid of CD86-mEos4b and CTLA4-mEos4b were transfected into HEK293T cells in 6-well plates at ~60% confluence with Lipofectamine 3000 (Thermo Fisher Scientific) according to the manufacturer's instructions. After about 24 h, the cells were transferred on PLL-PEG-RGD coated cover glasses (35 × 64 mm, # 1.5, Thermo Fisher Scientific) using flexiPERM chambers. After about 16 h, cells were washed with 400 mM saccharose (Sigma-Aldrich) in PBS and fixed with 4% paraformaldehyde (Thermo Fisher Scientific), 0.1% glutaraldehyde (Sigma-Aldrich) and 400 mM saccharose in PBS buffer for 15 minutes. Then, cells were washed three times with sterile-filtered PBS. Gold particles (120 nm; Nanopartz, Loveland, CO, USA) were sonicated for 10 minutes and added in a 1:5 dilution in PBS to the cells for 8 minutes. Cells were washed again three times with PBS and PALM movies were recorded in sterile-filtered PBS.

MET-mEos4b cells were seeded on PLL-PEG-RGD coated cover glasses (35 × 64 mm, # 1.5, Thermo Fisher Scientific) at a density of $(2 - 2.5) \cdot 10^4$ cells/well using 8-well flexiPERMs (Sarstedt, Nümbrecht, Germany). After approximately 16-24 h, the cells were washed once with serum-free imaging medium containing DMEM with 1% GlutaMAX and 50 mM HEPES buffer (pH 7.2–7.5; Gibco, Life Technologies, CA, USA) and incubated in serum-free imaging medium for approximately 4 hours. Afterwards, cells were incubated at 4° C for 5 min. Either HGF, $InlB_{321}$-ATTO 647N or no ligand was added to the cells in concentrations of 1 nM or 5 nM, respectively, for 10 minutes at 4° C. After that, cells were washed with 400 mM saccharose (Sigma-Aldrich) and fixed with 4% paraformaldehyde (Thermo Fisher Scientific), 0.1% glutaraldehyde (Sigma-Aldrich) and 400 mM saccharose in PBS buffer for at least 15 minutes. Then, cells were washed three times with sterile-filtered PBS. Gold particles (120 nm; Nanopartz, Loveland, CO, USA) were sonicated for 10 minutes and added in a 1:4 solution in PBS to the cells for 10 minutes. Cells were washed again three times with PBS and PALM movies were recorded in sterile-filtered PBS.

(q)PALM imaging of mEos4b, CD86-mEos4b, CTLA4-mEos4b and MET-mEos4b

Quantitative PALM movies were recorded using a custom-built widefield setup equipped with an inverted microscope (Olympus IX71). The microscope was equipped with an 100x oil immersion objective (PlanApo 100 × TIRFM, NA≥1.45, Olympus) and a nose piece for drift minimization. Lasers with the wavelength of 405 nm (LBX-405-50-CSB-PP, Oxxius, 0–30 mW/cm²), 568 nm (Sapphire 568 LP, Coherent, 0.21 kW/cm²) and 638 nm (LBX-638-180, Oxxius, 4.6 W/cm²) were coupled into the objective and movies were recorded with total internal reflection (TIR) illumination. Bandpass filters (ET 700/75; BrightLine HC 590/20, AHF) were used to filter the emission light. SMLM movies of 15,000–40,000 frames were recorded with an EMCCD camera (iXon Ultra, Andor) with a physical pixel size of 157 nm (camera pixel and magnification), an exposure time of 100 ms, and an EM gain of 200 until almost no blinking was observed. For each condition a minimum of ten cells from at least three different measuring days were used for data analysis.

(q)PALM data analysis

Single-molecule localizations were filtered using rapidSTORM (v.3.3) (Wolter et al., 2010)Klicken oder tippen Sie hier, um Text einzugeben.. The super-resolved images were loaded into Fiji (Schindelin et al., 2012) and cell areas were determined. Single clusters per cell were analyzed with the 3D Object counter v2.0 (Bolte and Cordelières, 2006) with a threshold of 125 and a minimum size filter of 10. Receptor densities were obtained from 21 cells by dividing the total number of clusters by the respective cell area. The error is given as standard deviation.

Detailed protocols for the data analysis of qPALM movies have been presented (Krüger et al., 2017; Baldering et al., 2019b; Karathanasis et al., 2020). Briefly, PALM images were generated with rapidSTORM (v3.3) and localizations of consecutive frames were grouped with a distance threshold of 90 nm. Furthermore, LocAlization Microscopy Analyzer (LAMA) (Malkusch and Heilemann, 2016) was used to extract the number of blinking events of single localization clusters in the super-resolved images. Since individual cells do not contain enough statistics, we randomly mixed the data of each condition ten times and analyzed 80 percent of the respective data. Histograms of the relative frequency of number of blinking events were plotted and fitted with the qSMLM software (Baldering et al., 2019a) yielding the corrected monomer/dimer fractions. The mean values were determined for each condition and the error is given as standard deviation.

The q-value obtained from the blinking histogram of CTLA4-mEos4b was converted into the detection efficiency (d) according to the following equation (1):

$$d = \frac{2-2q}{2-q} \quad (1)$$

SPT sample preparation and imaging of MET-mEos4b

MET-mEos4b cells were seeded on PLL-PEG-RGD coated round cover glasses at a density of $(20 - 30) \cdot 10^4$ cells/well in 6-well plates. After approximately 24 h, the round cover glasses were transferred into custom-built holders. The cells were washed once with serum-free imaging medium containing DMEM with 1% GlutaMAX and 50 mM HEPES buffer (pH 7.2–7.5; Gibco, Life Technologies). In the presence of ligands, either HGF or $InlB_{321}$-ATTO647N was added to the cells at a concentration of 1 nM in imaging medium. sptPALM and uPAINT measurements were performed using a commercial microscope (N-STORM, Nikon). The microscope was equipped with a 100x objective (100 × Apo TIRF oil, 1.49 NA), a 647 nm laser (0.2 kW/cm^2), a 561 nm laser (0.2 kW/cm^2), a 405 nm laser (0-38 mW/cm^2) and was operated with TIR illumination. Image acquisition was controlled by µManager (version 1.4.20) (Edelstein et al., 2014) and NIS-Elements (version 4.30.02, Nikon, Düsseldorf, Germany) using an exposure time of 20 ms and an EM gain of 300. sptPALM or uPAINT movies were recorded with an EMCCD camera (DU-897U-CS0-BV; Andor Technology, Belfast, UK), using a physical pixel size (camera and magnification) of 158 nm. Recorded movies had a length of 1,000 frames. For each condition about 20 cells from at least three different days were used for data analysis.

SPT data analysis

The data analysis of sptPALM measurements was performed with a plugin for MetaMorph (version 7.7.0.0, Molecular Devices, Sunnyvale, USA), called PALM-Tracer (Bordeaux Imaging Center, France) (see also (Harwardt et al., 2017)). Localizations were determined by centroid fitting and connected into trajectories if the distance between two subsequent localizations did not exceed 5 pixels (790 nm). MSD values were calculated from these trajectories and diffusion coefficients were determined by fitting the first four points of the MSD plot. MSD data were also used in diffusion type analysis. Based on the dynamic localization precision the smallest determinable diffusion coefficient D_{min} (0.008 µm²/s) was calculated and all diffusion coefficients $d \leq D_{min}$ were assigned as immobile. Further analyses (Rossier et al., 2012) were used to differentiate between confined and free diffusion applying a τ value of 60 ms as threshold. Statistical analysis of diffusion coefficients and diffusion types was performed in Origin (OriginPro 2016G, OriginLab).

Supplemental References

Bolte S, Cordelières FP (2006). A guided tour into subcellular colocalization analysis in light microscopy. J Microsc 224, 213–232.

Edelstein AD, Tsuchida MA, Amodaj N, Pinkard H, Vale RD, Stuurman N (2014). Advanced methods of microscope control using μManager software. J Biol Methods 1.

Krüger C, Fricke F, Karathanasis C, Dietz MS, Malkusch S, Hummer G, Heilemann M (2017). Molecular counting of membrane receptor subunits with single-molecule localization microscopy. In: Jörg Enderlein, Ingo Gregor, Zygmunt K. Gryczynski, Rainer Erdmann und Felix Koberling (Hg.). SPIE BiOS. San Francisco, California, United States, Saturday 28 January 2017: SPIE (SPIE Proceedings), 100710K.

Malkusch S, Heilemann M (2016). Extracting quantitative information from single-molecule super-resolution imaging data with LAMA - LocAlization Microscopy Analyzer. Sci Rep 6, 34486.

Schindelin J, Arganda-Carreras I, Frise E, Kaynig V, Longair M, Pietzsch T, Preibisch S, Rueden C, Saalfeld S, Schmid B, Tinevez J-Y, White DJ, Hartenstein V, Eliceiri K, Tomancak P, Cardona A (2012). Fiji. An open-source platform for biological-image analysis. Nat Methods 9, 676–682.

Wolter S, Schüttpelz M, Tscherepanow M, van de Linde S, Heilemann M, Sauer M (2010). Real-time computation of subdiffraction-resolution fluorescence images. J Microsc 237, 12–22.